Springer

Acta Mechanica Sinica

CrossMark click for updates

• RESEARCH PAPER •

Acta Mech. Sin., Vol. 39, 322399 (2023)
https://doi.org/10.1007/s10409-022-22399-x

A modified method considering vortex effect for modelling unsteady cavitating flows

Bojie Hong, Changli Hu*, and Haojie Xing

School of Energy and Power Engineering, Nanjing University of Science and Technology, Nanjing 210094, China

Received November 6, 2022; accepted November 19, 2022; published online January 16, 2023

The objective of this study is to propose a modified method for the cavitation model and turbulence model, accounting for the influence of vortex motion on unsteady cavitating flows. A function of the ratio of strain rate tensor and rotation rate tensor is introduced into the Zwart cavitation model and the shear stress transfer (SST) γ-$Re_{\theta t}$ turbulence model respectively. The modified method is applied to simulate the unsteady cloud cavitating flow around Clark-Y hydrofoil and evaluated by the experimental data. The results show that the modified model can better capture the unsteady process of the cloud cavity, especially the fully developed attached cavity and the large-scale cloud shedding behaviors. These benefit from the increase of turbulent dissipation rate per unit energy and the evaporation rate of the modified method. In addition, the lift coefficient fluctuation in time and the time-averaged u-velocity profiles predicted by the modified model are better agreement with the experimental results.

Vortex motion, Cavitation model, Turbulent eddy viscosity, Unsteady cavitating flows

Citation: B. Hong, C. Hu, and H. Xing, A modified method considering vortex effect for modelling unsteady cavitating flows, Acta Mech. Sin. **39**, 322399 (2023), https://doi.org/10.1007/s10409-022-22399-x

1. Introduction

Cavitation is an important hydrodynamic phenomenon, which commonly occurs in various hydraulic machinery, and is often accompanied by material damage, vibration, and noise [1,2]. For a long time, the cavitation phenomenon has received great attention. It is well known that cavitating flows include almost all complex flow problems such as turbulence, phase transition and compressibility [3]. Among them, cavitation can be induced in the vortex structures, and the unsteady cavity is always accompanied by the motion and transport of vortices [4], which brings great challenges to the numerical simulation of cavitation.

Nowadays, many researchers found that the unsteady cavity evolution is closely related to vortex motion [5,6]. On the one hand, cavitation would change the vortex characteristics in the flow field. The research of Kubota et al. [7] showed that a vorticity extremum was observed at the center of the cavitation cloud. Similarly, the collapse process of the cavitation cloud was proved to be a major source of vorticity production [8]. Ohta and Sugiura [9] found that vortex cavitation weakened the turbulence vortex maintenance mechanism and decreased the friction coefficient. Some studies pointed out that cavitation could affect the vortex characteristics, such as promoting vortex production [10], enhancing the tip clearance vortex intensity [11] and increasing vortex shedding frequency [12]. Moreover, it was found that the cavity evolution significantly altered the interaction between the leading and trailing edge vortices [13], and the U-shaped and O-shaped vortex structures would be produced during the cavity shedding process [14]. However, other researchers pointed out that the abundant vortex structures could also affect the inception and development of cavitation. Katz and O'Hern [15] experimentally observed the cavitation phenomena behind a sharp-edged plate. They found the streamwise vortices were the main contributor to cavitation inception. This conclusion could be supported by the research of Avrahami et al. [16]. Similarly,

*Corresponding author. E-mail address: changlihu@njust.edu.cn (Changli Hu)
Executive Editor: Xueming Shao

Altimira and Fuchs [17] confirmed that the local pressure inside vortex cores would decrease to enhance the production of cavitation in the flow of a throttle geometry. In addition, it was reported that the vortex stretching behavior could promote cavity development, breakup, and collapse [18,19]. Consequently, the complex interactions between cavitation and the vortex motion indeed make the numerical simulation of cavitating flows to be challenging.

In recent years, the numerical method based on the Navier-Stokes equation has been widely used [20-22], which is generally coupled with the multiphase flow model, cavitation model, and turbulence model. Many studies [23-26] indicated that large eddy simulation (LES) could capture the vortex structure well and significantly improve the prediction accuracy of cavitation. However, LES is sensitive to the grid level. Also, most models cannot accurately reproduce the vortex features in turbulent flow [27], resulting in an inaccurate prediction of the phase transition process and eddy viscosity. Therefore, many scholars are devoted to the modification work of the numerical model. For the modification of the turbulence model, an effective approach is to modify the turbulence production term, and then control the turbulent eddy viscosity in the vortex core region. Spalart and Shur [28] applied the function of strain rate and rotation rate to the production term of Spalart-Allmaras (SA) model, which significantly improved the simulation of rotating/curved channel flows. Inspired by this research, some scholars applied the similar modified method to the two-equation models, such as the production terms of the shear stress transfer (SST) model [29], the k production term of the standard k-ε model [30], and the ω production term of Wilcox k-ω mode [31]. Their results showed that the modified turbulence model could better capture the rotation effect and improve the prediction for cavitating flows. Similarly, Ye et al. [32] considered the effect of surface curvature on cavity evolution and proposed a new partially-averaged Navier-Stokes (PANS) turbulence model based on the modified SST model. The results confirmed its good applicability. On the other hand, there are also some modification works of the cavitation model. Guo [33] established the quantitative relationship between the vortex identification parameter and the condensation coefficient of the Zwart cavitation model. The modified cavitation model realized the reasonable prediction for the tip leakage vortex (TLV) cavitation. Le and Tran [34] introduced an additional pressure term caused by the vortices into the Saito cavitation model [35] to modify the phase-change pressure threshold. They found that this method can effectively improve the prediction of cavity structures. In addition, based on the concept of cavitation vortex, Zhao et al. [36] proposed a cavitation model considering the effect of cavitation-vortex interaction on the interphase mass transfer process. Cheng et al. [37] considered the strong attraction of the tip vortex (TV) to non-condensable gas bubbles, and proposed a new Euler-Lagrangian cavitation model based on the Rayleigh-Plesset equation. The new model can provide a more accurate prediction for tip vortex cavitation (TVC).

The above studies show that the modification of the turbulence model or cavitation model can improve the prediction of cavitating flows, yet only one of them is done for most literatures. Actually, due to the cavitation-vortex interaction, the simultaneous modification of the turbulence model and cavitation model is of great significance for the accurate prediction of cavity evolution. As a result, we try to modify the phase-change coefficients of the Zwart cavitation model and the ω production term of SST γ-$Re_{\theta t}$ turbulence model by introducing different governing functions. In the present paper, Sect. 2 describes the numerical method. In Sect. 3, the modified model is used to simulate the cloud cavitating flow around the two-dimensional (2D) Clark-Y hydrofoil. Finally, the main conclusions are summarized in Sect. 4.

2. Numerical method

2.1 Continuity and momentum equations

The phases of liquid and vapor are assumed to be continuous, and the two phases are in thermal equilibrium and uniformly mixed. The governing equations of mass continuity and momentum are given below:

$$\frac{\partial \rho}{\partial t}+\frac{\partial(\rho u_j)}{\partial x_j}=0, \tag{1}$$

$$\frac{\partial(\rho u_i)}{\partial t}+\frac{\partial(\rho u_i u_j)}{\partial x_j}=-\frac{\partial p}{\partial x_i}+\frac{\partial}{\partial x_j}\left(\mu\frac{\partial u_i}{\partial x_j}\right). \tag{2}$$

The mixture density ρ and mixture viscosity μ can be expressed as

$$\mu=\alpha_{\mathrm{v}}\mu_{\mathrm{v}}+(1-\alpha_{\mathrm{v}})\mu_{\mathrm{l}}, \tag{3}$$

$$\rho=\alpha_{\mathrm{v}}\rho_{\mathrm{v}}+(1-\alpha_{\mathrm{v}})\rho_{\mathrm{l}}, \tag{4}$$

where p is the mixture pressure, subscripts i and j represent the directions of flow velocity, subscripts v and l represent the vapor phase and liquid phase, and α_{v} is the vapor volume fraction.

2.2 Cavitation model

2.2.1 *Zwart cavitation model*

The Zwart cavitation model [38] is based on the simplified form of the Rayleigh-Plesset equation, and the mass transfer equation is given as follows:

$$\frac{\partial(\rho_{\mathrm{v}}\alpha_{\mathrm{v}})}{\partial t}+\frac{\partial(\rho_{\mathrm{v}}\alpha_{\mathrm{v}}u_j)}{\partial x_j}=m^{+}-m^{-}. \tag{5}$$

The source terms can be defined as

$$m^{+}=F_{\mathrm{vap}}\frac{3\alpha_{\mathrm{nuc}}(1-\alpha_{\mathrm{v}})\rho_{\mathrm{v}}}{R_{\mathrm{B}}}\sqrt{\frac{2(P_{\mathrm{v}}-P)}{3\rho_{1}}},\quad P\le P_{\mathrm{v}}, \tag{6}$$

$$m^{-}=F_{\mathrm{cond}}\frac{3\alpha_{\mathrm{v}}\rho_{\mathrm{v}}}{R_{\mathrm{B}}}\sqrt{\frac{2(P-P_{\mathrm{v}})}{3\rho_{1}}},\quad P>P_{\mathrm{v}}, \tag{7}$$

where m^{+} and m^{-} represent the evaporation and condensation rates respectively. The vaporization coefficient F_{vap} = 50, and the condensation coefficient F_{cond} = 0.01. The nucleation volume fraction $\alpha_{\mathrm{nuc}}=5\times10^{-4}$, bubble radius $R_{\mathrm{B}}=10^{-6}$ m, and P_{v} is the saturation vapor pressure.

2.2.2 Modified Zwart model

Due to the vortices promoting the development of cavities, the modification function min(r^2, 1) in Ref. [27] is introduced to modify the evaporation and condensation coefficients of the Zwart cavitation model:

$$F_{\mathrm{vapNEW}}=\frac{F_{\mathrm{vap}}}{\min\left(r^{2},1\right)}, \tag{8}$$

$$F_{\mathrm{condNEW}}=F_{\mathrm{cond}}\cdot\min(r^{2},1), \tag{9}$$

$$r=\frac{S}{\Omega}, \tag{10}$$

$$S^{2}=2S_{ij}S_{ij},\quad \Omega^{2}=2\Omega_{ij}\Omega_{ij}, \tag{11}$$

$$S_{ij}=\frac{1}{2}\left(\frac{\partial u_{i}}{\partial x_{j}}+\frac{\partial u_{j}}{\partial x_{i}}\right),\quad \Omega_{ij}=\frac{1}{2}\left(\frac{\partial u_{i}}{\partial x_{j}}-\frac{\partial u_{j}}{\partial x_{i}}\right), \tag{12}$$

where F_{vapNEW} and F_{condNEW} are the modified evaporation coefficient and condensation coefficient; S_{ij} and Ω_{ij} represent the components of the strain rate tensor and rotation rate tensor respectively.

When $\Omega > S$, $r < 1$, the vortex motion is dominant (the flow is in the vortex region), and the evaporation and condensation coefficients need to be modified. When $\Omega < S$, $r > 1$, the vortex motion is weak, and the original coefficients are maintained. The modified Zwart cavitation model can increase the evaporation rate while reducing the condensation rate in the vortex region.

2.3 Turbulence model

2.3.1 SST γ-$Re_{\theta t}$ turbulence model

The SST γ-$Re_{\theta t}$ turbulence model proposed by Menter et al. [39] is based on the SST k-ω model [40], coupled with the two equation γ-$Re_{\theta t}$ transition model including the intermittency and the transition onset momentum thickness Reynolds number.

The intermittency equation is as follows:

$$\frac{\partial(\rho\gamma)}{\partial t}+\frac{\partial(\rho u_{j}\gamma)}{\partial x_{j}}=\frac{\partial}{\partial x_{j}}\left[\left(\mu+\frac{\mu_{t}}{\sigma_{\gamma}}\right)\frac{\partial\gamma}{\partial x_{j}}\right]+P_{\gamma1}-E_{\gamma1}+P_{\gamma2}-E_{\gamma2}, \tag{13}$$

$$P_{\gamma1}=2F_{\mathrm{length}}\rho S[\gamma F_{\mathrm{onset}}]^{c_{a1}},\quad E_{\gamma1}=c_{e1}P_{\gamma1}\gamma, \tag{14}$$

$$P_{\gamma2}=(2c_{a2})\rho\Omega\gamma F_{\mathrm{turb}},\quad E_{\gamma2}=c_{e2}P_{\gamma2}\gamma, \tag{15}$$

where γ is the intermittent factor, S is the strain rate, Ω is the vorticity, F_{length} is used to adjust the length of the transition region, F_{onset} and F_{turb} are the functions to control the transition process, c_{a1}, c_{e1}, c_{a2}, and c_{e2} are the constants for the intermittency equation with the values of 0.5, 1.0, 0.03, and 50, respectively.

The transport equation for the transition momentum thickness Reynolds number $Re'_{\theta t}$ is as follows:

$$\frac{\partial\left(\rho Re'_{\theta t}\right)}{\partial t}+\frac{\partial\left(\rho u_{j}Re'_{\theta t}\right)}{\partial x_{j}}=P_{\theta t}+\frac{\partial}{\partial x_{j}}\left\{\sigma_{\theta t}\left[(\mu+\mu_{t})\frac{\partial Re'_{\theta t}}{\partial x_{j}}\right]\right\}, \tag{16}$$

$$P_{\theta t}=c_{\theta t}\frac{\rho}{t}(Re_{\theta t}-Re'_{\theta t})(1.0-F_{\theta t}), \tag{17}$$

where the source term $P_{\theta t}$ is intended to force $Re'_{\theta t}$ to match the empirically correlated transition momentum thickness Reynolds number $Re_{\theta t}$, t is a time scale, $F_{\theta t}$ is the mixing function used to allow $Re'_{\theta t}$ to diffuse in from the freestream, and the model constants $c_{\theta t}$ = 0.03, $\sigma_{\theta t}$ = 10.

The modified k equation is obtained by coupling the γ-$Re_{\theta t}$ transition model with the SST k-ω turbulence model:

$$\frac{\partial(\rho k)}{\partial t}+\frac{\partial(\rho k u_{j})}{\partial x_{j}}=\frac{\partial}{\partial x_{j}}\left[\left(\mu+\frac{\mu_{t}}{\sigma_{k}}\right)\frac{\partial k}{\partial x_{j}}\right]+P'_{k}-D'_{k}, \tag{18}$$

$$P'_{k}=\gamma_{\mathrm{eff}}P_{k},\quad D'_{k}=\min\left[\max(\gamma_{\mathrm{eff}},0.1),1.0\right]D_{k}. \tag{19}$$

The ω equation is consistent with the original SST k-ω model:

$$\frac{\partial(\rho\omega)}{\partial t}+\frac{\partial(\rho\omega u_{j})}{\partial x_{j}}=\frac{\partial}{\partial x_{j}}\left[\left(\mu+\frac{\mu_{t}}{\sigma_{\omega}}\right)\frac{\partial\omega}{\partial x_{j}}\right]+p_{\omega}-D_{\omega}+Cd_{\omega}, \tag{20}$$

where P'_{k} and D'_{k} are respectively the generation and destruction terms of the turbulent kinetic energy equation in the SST γ-$Re_{\theta t}$ model, and γ_{eff} is the effective intermittency.

2.3.2 Modified SST γ-$Re_{\theta t}$ model

In Eq. (20), ω is referred to as the specific dissipation rate, which is the rate of turbulent dissipation per unit energy [41]. The ω production term of the original SST γ-$Re_{\theta t}$ model can be given by

$$p_{\omega}=\frac{\alpha}{\nu_{t}}p_{k}. \tag{21}$$

However, the original SST γ-$Re_{\theta t}$ model does not consider the effect of vortex motion on cavitation, which caused the viscosity prediction and cavity collapse rate are much larger in the vortex region. Therefore, in this study, the modification function min(r^2, 1) is introduced in the P_{ω} item of SST γ-$Re_{\theta t}$ model, meanwhile, an empirical coefficient C is

added in the following modification function:

$$p_{\omega\mathrm{NEW}} = \frac{p_\omega}{\min\left(Cr^2, 1\right)}, \tag{22}$$

where $P_{\omega\mathrm{NEW}}$ is the modified ω production term, and the empirical coefficient $C = 0.5$.

The modified SST γ-$Re_{\theta t}$ turbulence model strengthens the ω production term to increase the turbulent dissipation rate per unit of energy in the vortex region, which can reduce the turbulent eddy viscosity and vortex dissipation rate. As a result, it is supposed that the cavity will not collapse over quickly. The modified SST γ-$Re_{\theta t}$ turbulence model and Zwart cavitation model are called as the modified model in the following.

2.4 Boundary conditions and grid generation

Figure 1 shows the computational domain and boundary conditions. The Clark-Y hydrofoil is with an angle of attack of 8°, and the chord length is $c = 0.07$ m. Cavitating flows were simulated based on the calculation plat ANSYS CFX 19.0. The length and height of the computational domain are 10.7c and 2.9c respectively. The inlet velocity is set to be U = 10 m/s, and the outlet pressure is adjusted so that the computation can be performed with the cavitation number σ = 0.8. The fluid for numerical calculation is water and water vapor at 25 , and the saturated vapor pressure is P_v = 3169 Pa. In addition, the upper and lower boundaries are set as free-slip walls, the hydrofoil surface is no-slip wall boundaries, and the front and rear boundaries are set as symmetry.

The computational domain consists of the hexahedral structured grid, and the grids in the near-wall region of the hydrofoil are refined, as shown in Fig. 2. To reduce the effect of grid density on cavitation simulation, Table 1 shows the time-averaged lift and drag coefficients of Clark-Y hydrofoil for different grid densities. It can be seen that the values of lift and drag coefficients for the Mid-size 2 trend to consist with that of the fine gird. Then considering the economy of calculation, the grid of Mid-size 2 is selected in the present study.

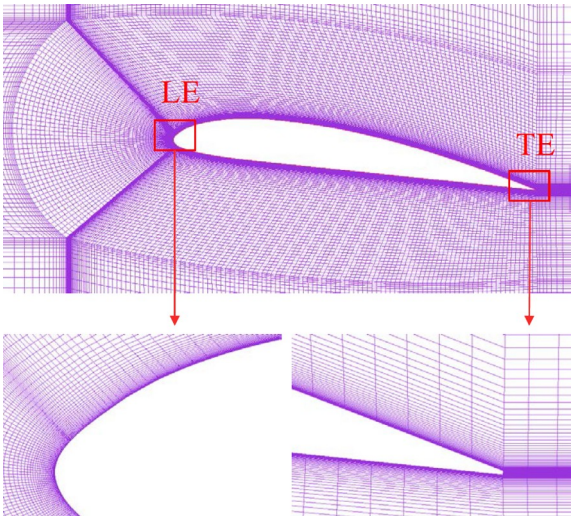

Figure 2 Grid generation and refinement around the Clark-Y hydrofoil.

Table 1 Time-averaged lift and drag coefficients under different grid densities

Grid size	Nodes	$\overline{C_l}$	$\overline{C_d}$
Coarse	405240	0.708	0.104
Mid-size 1	619740	0.700	0.101
Mid-size 2	850080	0.689	0.101
Fine	1134800	0.686	0.102

3. Results and discussion

The time-evolution process of the cavity for the different numerical methods and the experiment [42] is shown in Fig. 3. Here, the original model represents the original Zwart cavitation model and SST γ-$Re_{\theta t}$ turbulence model before modification. The results demonstrate that the two models can predict the unsteady process of the cavity around the hydrofoil, including the cavity inception, development, break-off, and shedding. However, the modified model can better capture the large-scale cloud cavity shedding from the trailing edge, as shown at t_0 and $t_0 + T$. In addition, the attached cavity predicted by the modified model can grow to the trailing edge of the hydrofoil, and the breakup and shedding process of the cavity agrees well with the

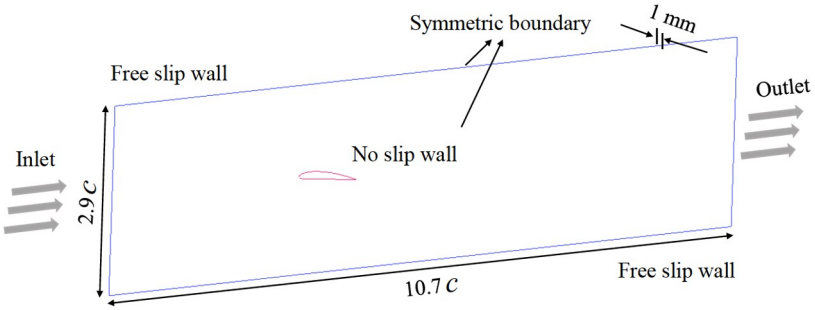

Figure 1 Computational domain and boundary conditions.

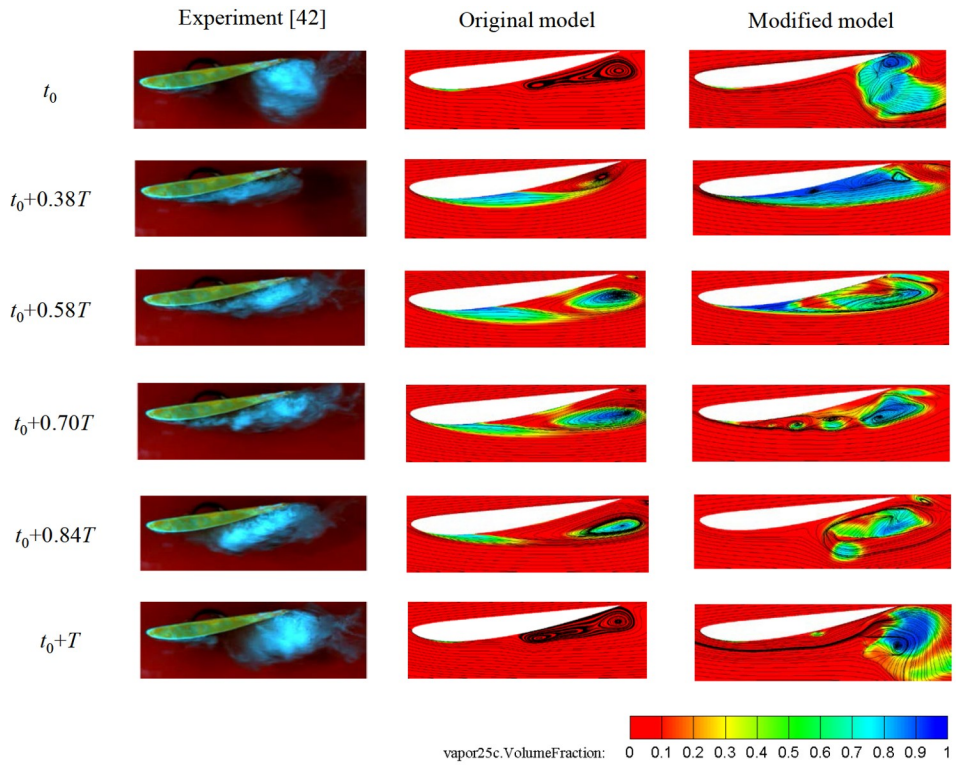

Figure 3 Instantaneous vapor volume fraction contours and streamlines with different models.

experimental results, as shown at t_0 + 0.38T-0.84T.

In order to further study the differences of cloud cavity evolution for the two numerical models, Fig. 4 shows the temporal and spatial variation of vapor volume fraction on the hydrofoil suction surface. The y-axis is the non-dimensional position along the chord, and the x-axis is the non-dimensional time, where T_{ref} is defined as $T_{\text{ref}} = c/U$. It can be found that the cavities predicted by the two models evolve periodically, but the evolution period for the modified model is shorter than that of the original model. Besides, the cavity obtained by the modified model is slender and continuous along the y-axis direction, indicating that the attached cavity can cover the hydrofoil suction surface, which is consistent with the experiment as shown in Fig. 3. Furthermore, the modified model can capture more abundant cavity shedding behaviors near the trailing edge.

The time-averaged streamwise velocity distributions along the y-direction at the specified chordwise locations are displayed in Fig. 5. It can be found that the results of the modified model at the x/c = 0.4 and x/c = 0.6 agree better with the experimental data [42]. The original model underestimates the cavity thickness, resulting that the velocity along the y-direction grows faster than the experimental data. However, there are also some deficiencies in the

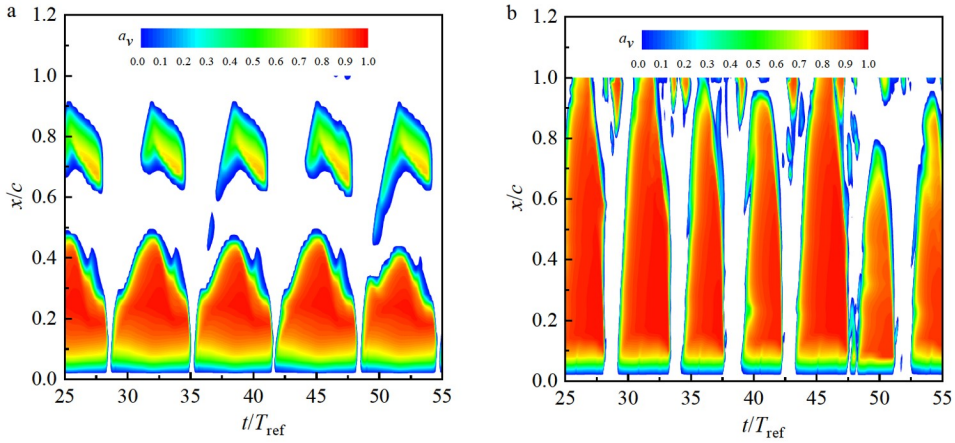

Figure 4 Time evolution of vapor volume fraction on the hydrofoil suction surface. **a** Original model; **b** modified model.

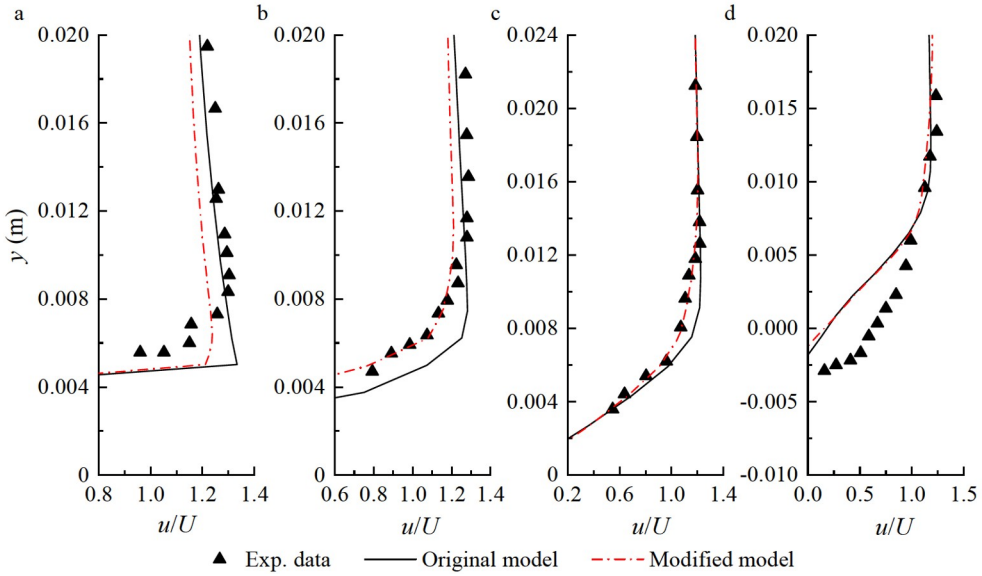

Figure 5 Time-averaged *u*-velocity component profiles with experiment and different models. **a** $x/c = 0.2$; **b** $x/c = 0.4$; **c** $x/c = 0.6$; **d** $x/c = 0.8$.

simulation results at $x/c = 0.2$ and $x/c = 0.8$. To make further analysis, as shown in Fig. 3, the cavity is rather thin at $x/c = 0.2$ and the large-scale shedding cavity occurs near the location of $x/c = 0.8$. These cavity behaviors are no doubt to increase the measurement difficulties of the particle image velocimetry (PIV) technology. Besides, a similar phenomenon can also be found in the studies of Huang et al. [42] and Hu et al. [43]. So it is supposed that the numerical results are reasonable due to the insufficient experimental measurements.

The hydrodynamic coefficient is also analyzed to discuss the prediction ability of the modified model as shown in Fig. 6. Figure 6a gives the time-evolution of lift coefficients and the corresponding time-averaged values. It can be seen that the modified model can capture more details of the pulsation, which is consistent with the experimental data [42]. Also, from the fast Fourier transform (FFT) results based on the lift coefficients in Fig. 6b, the dominant frequency of the lift coefficients predicted by the modified model and original model are $St = fc/U = 0.23$ and $St = 0.18$, respectively. That is to say, the modified model gives a slightly large frequency of the cavity evolution process, which is also illustrated in Fig. 4. Anyway, the predicted values of dominant frequency for the two models are reasonably consistent with the experimental data reported by Refs. [42,44]. Table 2 lists the time-averaged lift and drag coefficients as well as the frequencies obtained from the experiments and numerical calculations. By contrast, the modified model can predict the drag coefficient better than the original model. However, the modified model seems to underestimate the time-averaged lift coefficient. This may be due to the fact that the modified model can well capture

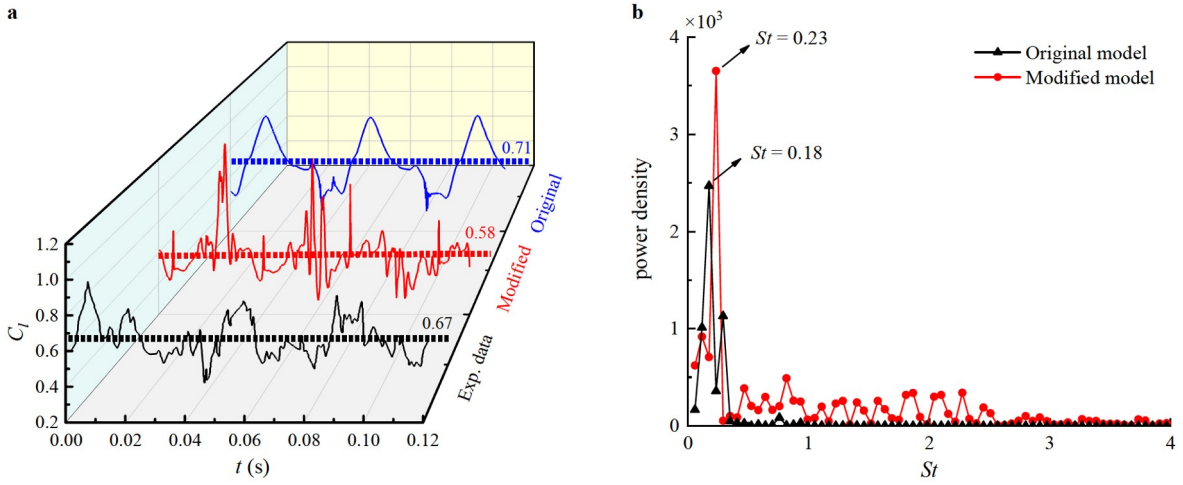

Figure 6 Time evolution of **a** lift coefficients and **b** FFT results.

Table 2 Comparison of the hydrodynamic characteristics with different models

Model	$\overline{C_l}$	$\overline{C_d}$	*St*
Exp. data [42]	0.67	–	0.22
Exp. data [44]	0.76	0.119	0.16
Original model	0.71	0.104	0.18
Modified PANS model [43]	0.66	0.131	0.21
Modified model	0.58	0.120	0.23

the time-evolution process of cavities, but the predicted scale of the cavity is smaller than that of the experiment, as shown in Fig. 3. This difference may make an impact on the pressure distribution of the suction side.

Figure 7 shows some instantaneous contours of the ω production term and turbulence eddy viscosity for the two numerical models. It is found that the ω production is mainly in the cavitation region, especially near the interface of water and vapor. This indicates that the phase changing process can induce large turbulent dissipation. By contrast, the modified model can significantly increase the ω production term in the cavitation region as expected. In addition, the modified model dramatically decreases the turbulent eddy viscosity in the cavitation region, which can strengthen unsteady behaviors of cavities to shed with a large scale.

Similarly, the evolutions of vorticity and cavitation source term for the two models are given in Fig. 8. Here, the positive and negative values in the cavitation source term contour represent the evaporation/condensation process, respectively. From the vorticity contours, the cavitation region is with the higher vorticity, and there are richer vortex structures captured by the modified model. Meanwhile, it is found that the positive vorticity interacts with the negative vorticity near the trailing edge, inducing complex large-scale vortex structures. Besides, compared with the original model, the modified model can increase the evaporation process in the cavitation region. Combined with the cavity evolution process in Fig. 3, it indicates that the modified model can promote the development of the cavity, and the massive evaporation source term in the trailing edge also ensures that the shedding cavitation cloud can last for a longer time.

4. Conclusions

In this paper, the influence of vortex motion on unsteady cavitating flows is considered. Different modified functions constructed by strain rate tensor and rotation rate tensor are introduced into the Zwart cavitation model and SST γ-$Re_{\theta t}$ turbulence model, so as to modify the phase-change coefficients of the cavitation model and the ω production term of the turbulence model, respectively. The modified model is used to simulate the cavitating flows around the 2D Clark-Y hydrofoil and evaluated by the experimental data. The following main conclusions are obtained:

(1) The modified model can well predict the unsteady evolution process of the cloud cavity around the hydrofoil, including the cavity inception, development, break-off, and shedding. Especially, the modified model can well capture

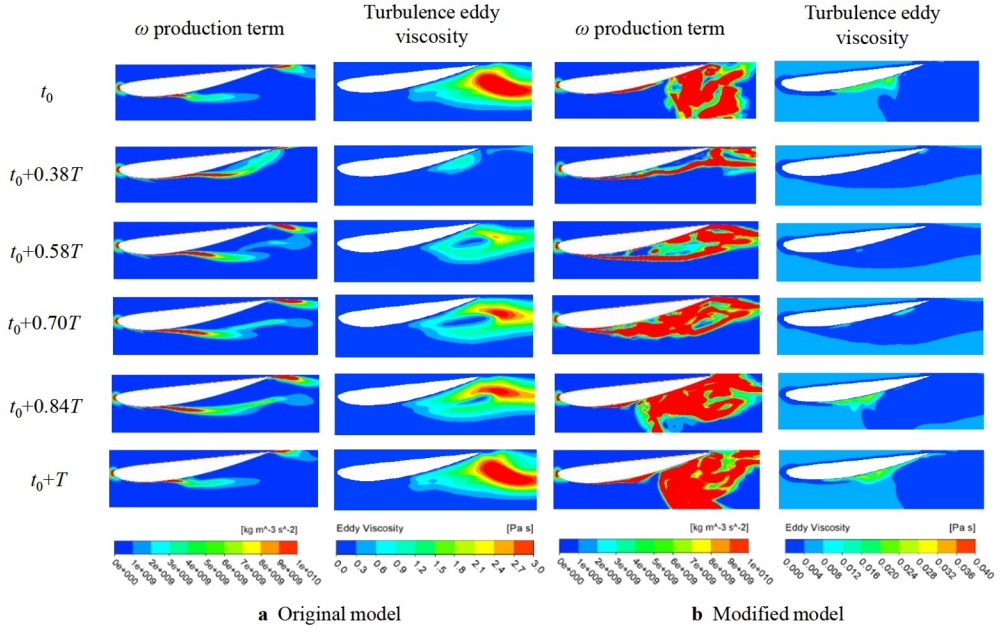

Figure 7 Time evolution of the ω production term and turbulence eddy viscosity with different models.

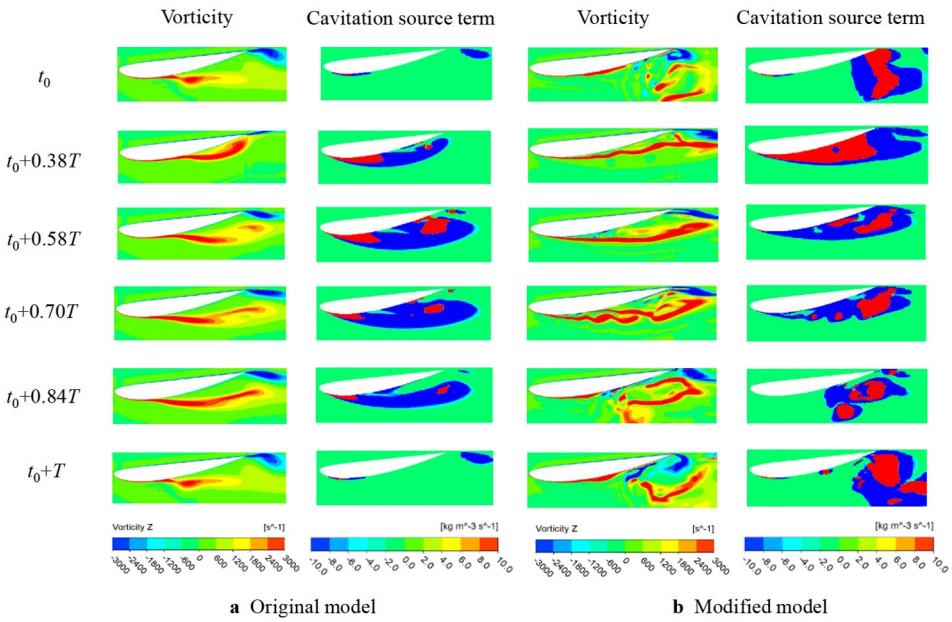

Figure 8 Time evolution of vorticity and cavitation source term with different models.

the large-scale cloud cavity shedding from the trailing edge. The time-averaged u-velocity profiles show that the modified model agrees better with the experiment. Also, the modified model can reasonably predict the hydrodynamic coefficients as well as the dominant frequency of unsteady behaviors of the cavity.

(2) The unsteady behaviors of the cloud cavity are relevant with the turbulent dissipation and the phase-changing process. The modified model increases the rate of turbulent dissipation per unit energy and the evaporation source term in the cavitation region as expected, which promotes the development of the cavity. Furthermore, the decrease of turbulent eddy viscosity and the supplement of evaporation source term ensure that the shedding large-scale cavitation cloud will not collapse over quickly.

Author contributions *Bojie Hong established the numerical method, made reasonable analysis and wrote the first draft of the manuscript. Changli Hu set the overall research goals, supervised the research activity execution and the final version revision. Haojie Xing helped process data and organize the manuscript.*

Acknowledgements *This work was supported by the National Natural Science Foundation of China (Grant No. 52076108).*

1 R. E. A. Arndt, Cavitation in fluid machinery and hydraulic structures, Annu. Rev. Fluid Mech. **13**, 273 (1981).
2 J. P. Franc, and J. M. Michel, Fundamentals of Cavitation (Springer, Netherlands, 2005).
3 B. Ji, H. Y. Cheng, B. Huang, X. W. Luo, X. X. Peng, and X. P. Long, Research progresses and prospects of unsteady hydrodynamics characteristics for cavitation, Adv. Mech. **49**, 201906 (2019).
4 Q. Guo, L. Zhou, Z. Wang, M. Liu, and H. Cheng, Numerical simulation for the tip leakage vortex cavitation, Ocean Eng. **151**, 71 (2018).
5 R. E. A. Arndt, Cavitation in vortical flows, Annu. Rev. Fluid Mech. **34**, 143 (2002).
6 B. Tian, J. Chen, X. Zhao, M. Zhang, and B. Huang, Numerical analysis of interaction between turbulent structures and transient sheet/cloud cavitation, Phys. Fluids **34**, 047116 (2022).
7 A. Kubota, H. Kato, H. Yamaguchi, and M. Maeda, Unsteady structure measurement of cloud cavitation on a foil section using conditional sampling technique, J. Fluids Eng. **111**, 204 (1989).
8 N. Dittakavi, A. Chunekar, and S. Frankel, Large eddy simulation of turbulent-cavitation interactions in a venturi nozzle, J. Fluids Eng. **132**, 121301 (2010).
9 T. Ohta, and R. Sugiura, Numerical prediction of interaction between turbulence structures and vortex cavitation, J. Turbul. **20**, 599 (2019).
10 B. Ji, X. Luo, R. E. A. Arndt, and Y. Wu, Numerical simulation of three dimensional cavitation shedding dynamics with special emphasis on cavitation-vortex interaction, Ocean Eng. **87**, 64 (2014).
11 C. Han, S. Xu, H. Cheng, B. Ji, and Z. Zhang, LES method of the tip clearance vortex cavitation in a propelling pump with special emphasis on the cavitation-vortex interaction, J. Hydrodyn. **32**, 1212 (2020).
12 P. Ausoni, M. Farhat, X. Escaler, E. Egusquiza, and F. Avellan, Cavitation influence on von Kármán vortex shedding and induced hydrofoil vibrations, J. Fluids Eng. **129**, 966 (2007).
13 B. Huang, Y. Zhao, and G. Wang, Large Eddy Simulation of turbulent vortex-cavitation interactions in transient sheet/cloud cavitating flows, Comput. Fluids **92**, 113 (2014).
14 J. Chen, B. Huang, T. Liu, Y. Wang, and G. Wang, Numerical investigation of cavitation-vortex interaction with special emphasis on the multistage shedding process, Appl. Math. Model. **96**, 111 (2021).
15 J. Katz, and T. J. O'Hern, Cavitation in large scale shear flows, J. Fluids Eng. **108**, 373 (1986).
16 I. Avrahami, M. Rosenfeld, S. Einav, M. Eichler, and H. Reul, Can vortices in the flow across mechanical heart valves contribute to cavitation? Med. Biol. Eng. Comput. **38**, 93 (2000).
17 M. Altimira, and L. Fuchs, Numerical investigation of throttle flow under cavitating conditions, Int. J. Multiphase Flow **75**, 124 (2015).
18 M. Liu, L. Tan, and S. Cao, Cavitation-vortex-turbulence interaction and one-dimensional model prediction of pressure for hydrofoil ALE15 by large eddy simulation, J. Fluids Eng. **141**, 021103 (2019).
19 M. G. D Giorgi, A. Ficarella, and D. Fontanarosa, in Active control of unsteady cavitating flows in turbomachinery: Proceedings of ASME Turbo Expo 2019, Turbomachinery Technical Conference and Exposition, Phoenix, 2019.
20 G. Wang, and M. Ostoja-Starzewski, Large eddy simulation of a

sheet/cloud cavitation on a NACA0015 hydrofoil, Appl. Math. Model. **31**, 417 (2007).
21 B. Ji, X. Luo, Y. Wu, X. Peng, and H. Xu, Partially-Averaged Navier–Stokes method with modified k-ε model for cavitating flow around a marine propeller in a non-uniform wake, Int. J. Heat Mass Transfer **55**, 6582 (2012).
22 P. K. Ullas, D. Chatterjee, and S. Vengadesan, Prediction of unsteady, internal turbulent cavitating flow using dynamic cavitation model, Int. J. Numer. Meth. Heat Fluid Flow **32**, 3210 (2022).
23 X. Long, H. Cheng, B. Ji, R. E. A. Arndt, and X. Peng, Large eddy simulation and Euler-Lagrangian coupling investigation of the transient cavitating turbulent flow around a twisted hydrofoil, Int. J. Multiphase Flow **100**, 41 (2018).
24 Y. Long, X. Long, B. Ji, and T. Xing, Verification and validation of large eddy simulation of attached cavitating flow around a Clark-Y hydrofoil, Int. J. Multiphase Flow **115**, 93 (2019).
25 Z. Wang, H. Cheng, and B. Ji, Euler-Lagrange study of cavitating turbulent flow around a hydrofoil, Phys. Fluids **33**, 112108 (2021).
26 A. Yu, W. Feng, and Q. Tang, Large Eddy Simulation of the cavitating flow around a Clark-Y mini cascade with an insight on the cavitation-vortex interaction, Ocean Eng. **266**, 112852 (2022).
27 X. Wang, and S. Thangam, Development and application of an anisotropic two-equation model for flows with swirl and curvature, J. Appl. Mech. **73**, 397 (2006).
28 P. R. Spalart, and M. Shur, On the sensitization of turbulence models to rotation and curvature, Aerosp. Sci. Tech. **1**, 297 (1997).
29 P. E. Smirnov, and F. R. Menter, Sensitization of the SST turbulence model to rotation and curvature by applying the Spalart-Shur correction term, J. Turbomach. **131**, 041010 (2009).
30 Y. Zhao, G. Y. Wang, and B. Huang, Applications of LSC turbulence model on unsteady cavitating flows, Chin. J. Appl. Mech. **31**, 1 (2014).
31 D. Y. Zhang, X. L. Li, Y. Yang, and Q. Zhang, Application of k-ω with P_ω enhancer turbulence model to delta wing vortical flows, Acta Aerodyn. Sin. **34**, 461 (2016).
32 W. Ye, Y. Yi, and X. Luo, Numerical modeling of unsteady cavitating flow over a hydrofoil with consideration of surface curvature, Ocean Eng. **205**, 107305 (2020).
33 Q. Guo, Study on Characteristics of the Blade Tip Leakage Vortex Flow and the Cavitating Flow Field (in Chinese), Dissertation for Doctoral Degree (China Agricultural University, Beijing, 2017).
34 A. D. Le, and H. T. Tran, Improvement of mass transfer rate modeling for prediction of cavitating flow, J. Appl. Fluid Mech. **15**, 551 (2022).
35 Y. Saito, R. Takami, I. Nakamori, and T. Ikohagi, Numerical analysis of unsteady behavior of cloud cavitation around a NACA0015 foil, Comput. Mech. **40**, 85 (2007).
36 Y. Zhao, G. Wang, and B. Huang, A cavitation model for computations of unsteady cavitating flows, Acta Mech. Sin. **32**, 273 (2016).
37 H. Cheng, X. Long, B. Ji, X. Peng, and M. Farhat, A new Euler-Lagrangian cavitation model for tip-vortex cavitation with the effect of non-condensable gas, Int. J. Multiphase Flow **134**, 103441 (2021).
38 P. J. Zwart, A. G. Gerber, and T. Belamri, in A two-phase flow model for predicting cavitation dynamics: Proceedings of International Conference on Multiphase Flow, Yokohama, 2004.
39 F. R. Menter, R. B. Langtry, S. R. Likki, Y. B. Suzen, P. G. Huang, and S. Volker, A correlation-based transition model using local variables—part I: Model formulation, J. Turbomach. **128**, 413 (2006).
40 F. R. Menter, Two-equation eddy-viscosity turbulence models for engineering applications, AIAA J. **32**, 1598 (1994).
41 D. C. Wilcox, Reassessment of the scale-determining equation for advanced turbulence models, AIAA J. **26**, 1299 (1988).
42 B. Huang, and G. Y. Wang, Experimental and numerical investigation of unsteady cavitating flows through a 2D hydrofoil, Sci. China Tech. Sci. **54**, 1801 (2011).
43 C. L. Hu, G. Y. Wang, G. H. Chen, and B. Huang, A modified PANS model for computations of unsteady turbulence cavitating flows, Sci. China-Phys. Mech. Astron. **57**, 1967 (2014).
44 G. Wang, I. Senocak, W. Shyy, T. Ikohagi, and S. Cao, Dynamics of attached turbulent cavitating flows, Prog. Aerosp. Sci. **37**, 551 (2001).

考虑旋涡效应的非定常空化流数值模型修正研究

洪伯杰, 胡常莉, 邢浩杰

摘要 本研究的目的是考虑旋涡运动对非定常空化流动的影响, 提出了一种空化模型和湍流模型的修正方法. 在Zwart空化模型和SST γ-$Re_{\theta t}$湍流模型中分别引入了由应变率张量和旋转率张量之比构建的函数. 将该修正方法用于模拟绕Clark-Y水翼的非定常云空化流动, 并通过与实验数据对比进行评估. 研究结果表明, 修正模型能够更好地捕捉到云空化的非定常过程, 特别是充分发展的附着空穴和大尺度的云空泡脱落行为. 这都得益于修正方法中单位能量的湍流耗散率和蒸发率的提高. 此外, 修正模型所预测的升力系数随时间的波动和时均流向速度分布与实验结果有较好的一致性.